



**HAL**  
open science

## Coaxial nanofibers of nickel/gadolinium oxide/nickel oxide as highly effective electrocatalysts for hydrogen evolution reaction

Heba El-Maghrabi, Amr Nada, Maged Bekheet, Stéphanie Roualdes, Wiebke Riedel, Igor Iatsunskyi, Emerson Coy, Aleksander Gurlo, Mikhael Bechelany

### ► To cite this version:

Heba El-Maghrabi, Amr Nada, Maged Bekheet, Stéphanie Roualdes, Wiebke Riedel, et al.. Coaxial nanofibers of nickel/gadolinium oxide/nickel oxide as highly effective electrocatalysts for hydrogen evolution reaction. *Journal of Colloid and Interface Science*, 2021, 587, pp.457-466. 10.1016/j.jcis.2020.11.103 . hal-03257767

**HAL Id: hal-03257767**

**<https://hal.science/hal-03257767v1>**

Submitted on 11 Jun 2021

**HAL** is a multi-disciplinary open access archive for the deposit and dissemination of scientific research documents, whether they are published or not. The documents may come from teaching and research institutions in France or abroad, or from public or private research centers.

L'archive ouverte pluridisciplinaire **HAL**, est destinée au dépôt et à la diffusion de documents scientifiques de niveau recherche, publiés ou non, émanant des établissements d'enseignement et de recherche français ou étrangers, des laboratoires publics ou privés.

# ***Coaxial nanofibers of nickel/ gadolinium oxide /nickel oxide as highly effective electrocatalysts for hydrogen evolution reaction***

*Heba H. El-Maghrabi <sup>a,b\*</sup>, Amr A. Nada <sup>a,c</sup>, Maged F. Bekheet <sup>d</sup>, Stéphanie Roualdes <sup>a</sup>, Wiebke Riedel <sup>e</sup>, Igor Iatsunskyi <sup>f</sup>, Emerson Coy <sup>f</sup>, Aleksander Gurlo <sup>d</sup>, Mikhael Bechelany <sup>a\*</sup>*

<sup>a</sup> *Institut Européen des Membranes, IEM–UMR 5635, ENSCM, CNRS, Univ Montpellier, Montpellier, France.*

<sup>b</sup> *Dept. of Refining, Egyptian Petroleum Research Institute, Cairo, Nasr city P.B. 11727, Egypt.*

<sup>c</sup> *Dept. of Analysis and Evaluation, Egyptian Petroleum Research Institute, Cairo, Nasr city P.B. 11727, Egypt.*

<sup>d</sup> *Fachgebiet Keramische Werkstoffe / Chair of Advanced Ceramic Materials, Institut für Werkstoffwissenschaften und -technologien, Technische Universität Berlin, Hardenbergstraße 40, 10623 Berlin, Germany.*

<sup>e</sup> *Institut für Chemie, Freie Universität Berlin, Arnimallee 22, 14195 Berlin, Germany*

<sup>f</sup> *NanoBioMedical Centre, Adam Mickiewicz University in Poznan, 3 Wszechnicy Piastowskiej str., 61-614, Poznan, Poland.*

*\*Corresponding author: [heba.el-maghrabi@ensicaen.fr](mailto:heba.el-maghrabi@ensicaen.fr) & [mikhael.bechelany@umontpellier.fr](mailto:mikhael.bechelany@umontpellier.fr)*

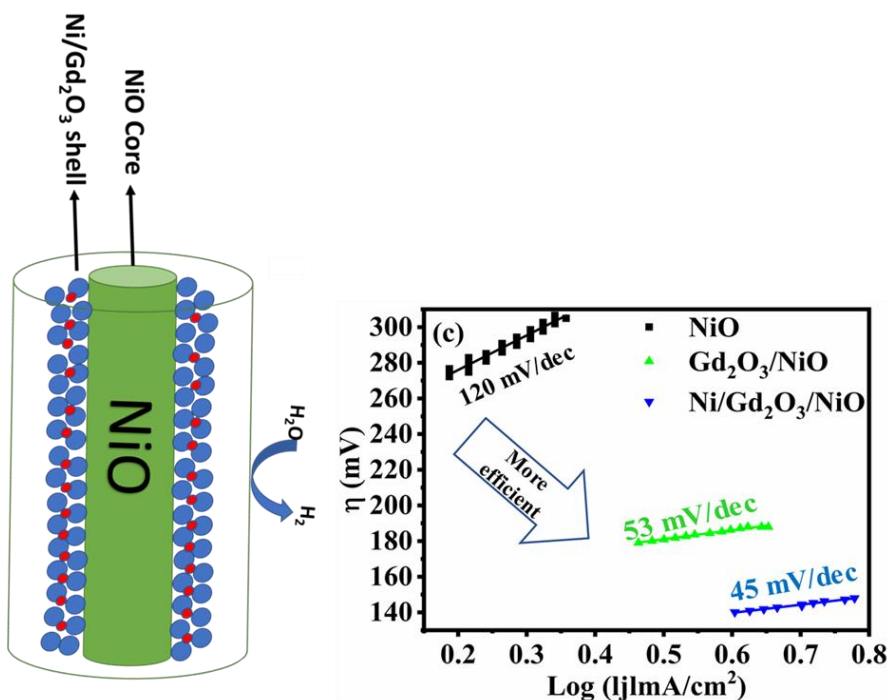
## **Abstract**

Cost-effective, active and stable electrocatalysts are pivotal to hydrogen production via electrocatalytic water splitting. Here we report on the preparation of novel nanofiber (NF) Ni/Gd<sub>2</sub>O<sub>3</sub>/NiO heterostructures by an electrospinning technique. The fabricated materials show high electrocatalytic performance for hydrogen evolution reaction (HER) with activities of onset potential at 89 mV, which is almost identical to that of platinum. The chemical and electronic properties of materials are successfully optimized in Ni/Gd<sub>2</sub>O<sub>3</sub>/NiO coaxial heterostructures; the NiO NF with Gd<sup>3+</sup> enhances remarkably its electrical conductivity and promotes HER reaction kinetics. It offers the distinct advantages of long-term durability and readiness for the integration into producing hydrogen via HER, affording better performance than benchmark Pt catalysts. The

successful fabrication of these metal oxides nanofibers and nanostructures may pave a new path for rational synthesis of efficient HER catalysts.

**Key words:** HER, Coaxial nanofibers, Ni/Gd<sub>2</sub>O<sub>3</sub>/NiO, Hydrogen generation, and water splitting.

**Graphical Abstract:**



### Highlights:

- Elaborated NiO nanofibers decorated with Ni/Gd<sub>2</sub>O<sub>3</sub> as coaxial structure.
- The Ni/Gd<sub>2</sub>O<sub>3</sub>/NiO has onset potential better than platinum electrode during the measurement of HER.
- The Ni/Gd<sub>2</sub>O<sub>3</sub>/NiO coaxial nanofibers have long-term durability during hydrogen generation.
- The highest exchange current density of Ni/Gd<sub>2</sub>O<sub>3</sub>/NiO up to 1.85 mA/cm<sup>2</sup> compared to most noble metal-free catalysis with decay of charge transfer resistance.

## 1. Introduction

In recent years, nickel oxide has been intensively studied for numerous applications, such as electrocatalysts [1-3], electrochemical capacitance [4-7] and for energy production [8]. All of that is mainly due to its particular properties as chemical, physical, specific electrochromic, thermoelectric and supercapacitance. Nickel oxide can be used in advanced technologies depending on its synthesis conditions and microstructures [9-16]. Many routes have been successfully applied to fabricate different NiO morphologies, including precipitation methods [17], hydrothermal [18, 19], solvothermal [20, 21], microemulsion [22, 23], oxidation of metallic Ni [24], thermal decomposition of Ni(II)- metalloorganic [25] and electrospinning [26-31].

Among these methods, the electrospinning has turned out to be a preferable choice because of its simplicity and scalability to yield nanofibers at an industrial level, and easy control over the morphology of the nanofibers [32-40]. Nickel oxide nanofiber morphology has gained significant attention due to the strong dependence of properties on the morphology [28, 41, 42]. The 1D nanofibers are easily modified *via* various approaches such as doping with heteroatoms, introducing strain in the basal plane, synergizing with conductive materials, coupling with the substrates of more active sites and defects to enhance the electrical conductivity and accelerating the kinetics of charge transfer [43-45]. These modification approaches could also be used to enhance the electrocatalytic performance of NiO NF as an ideal catalyst for energy production and, in specific, for the hydrogen evolution reaction (HER) *via* electrocatalytic water splitting [46]. One of the most significant challenges is the discovery of renewable, clean, safe, and sustainable energy sources to handle the expected shortage of non-renewable energies while controlling pollution. Hydrogen is a clean, zero carbon emission fuel when burned in oxygen. It is a promising approach as a renewable fuel for spacecraft, aircraft, vehicles, propulsion, and electric devices. Electrochemical water splitting is an effective and easy way of generating high-purity hydrogen. The most common HER electrocatalysts are using Pt metal with a high exchange current density and a near-zero overpotential [47]. However, Pt has many disadvantages like scarcity of supply, high cost, susceptibility to poisoning and a lack of durability of the catalyst. Despite the good electrocatalytic properties of Ni-based nanomaterials and nanofibers, few works in recent years have been conducted towards using these materials as alternative electrocatalysts for HER instead of Pt. For example, C@NiO/Ni nanofibers, prepared by electrospinning and a subsequent carbonization process, showed high effective and stable electrocatalytic for HER up to 22 hours

[48]. NiO and CrO<sub>3</sub> double surface-decorated Ni (Ni@ NiO@CrO<sub>3</sub>) nanofibers showed good electrocatalytic activity (100 mA cm<sup>-2</sup> at a low overpotential versus RHE at 228 mV) and superior stability (more than 120 h without decay) [49]. Yan and co-workers [50] reported an HER current of 5 mA cm<sup>-2</sup> at an overpotential of 110 mV with good stability for crystalline/amorphous core/shell Ni/NiO nanosheets. The good electrocatalytic activity of these nanosheets has been explained by the good conductivity of Ni nanoparticles on the surface of the fibers [49, 50]. Similarly, the embedding of Gd<sub>2</sub>O<sub>3</sub> and Gd particles was shown to enhance the electrocatalytic activity of Ni-Co alloy and Ni-CeO<sub>2</sub>-Gd electrodes to HER, respectively [51, 52]. Recently, we prepared self-supported carbon-Ni/NiO-Pd nanofiber electrodes for hydrogen and oxygen evolution reactions [53].

In the present work, we elaborate a novel Ni/Gd<sub>2</sub>O<sub>3</sub>/NiO coaxial heterostructures by an electrospinning technique. According to the best of our knowledge, no reports on such heterostructures for HER applications have been described so far. The nano-interfaces at Ni/NiO heterostructure is expected to enhance HER by stabilizing hydrogen atoms on metallic Ni and releasing the generated OH<sup>-</sup> on NiO site [2]. Moreover, the metallic Ni on the surface of the nanofibers facilitates the electron transfer. However, NiO/Ni heterostructures are not stable and exhibited high decay over time. Here, inspired by the fact that the addition of Gd<sub>2</sub>O<sub>3</sub> to Ni-based materials could increase their corrosion resistance and stability [54], we introduced Gd<sub>2</sub>O<sub>3</sub> to enhance the stability of Ni/NiO heterostructure. Moreover, the interaction between Gd<sub>2</sub>O<sub>3</sub> and NiO might generate new catalytic sites by alloying at the interfaces [55]. The fabricated electrocatalyst exhibits high electrocatalytic performance for hydrogen evolution reaction (HER) with activities of onset potential at 89 mV, which is almost identical to that of platinum. Moreover, Ni/Gd<sub>2</sub>O<sub>3</sub>/NiO offers the advantages of long-term durability after an accelerated scan of 5000 cycles as well as ready integration into an electrolyzes for HER, affording better performance than benchmark Pt catalysts.

## 2. Experimental

### 2.1. Materials

All the chemicals used were of analytical grade and used as received without further treatment. Nickel acetate (Ni(CH<sub>3</sub>COO)<sub>2</sub>.4H<sub>2</sub>O, 98%), gadolinium nitrate (Gd(NO<sub>3</sub>)<sub>3</sub>.6H<sub>2</sub>O, 99.9%), ethanol

(99.8%), dimethylformamide (DMF, 99.8%), poly(vinylpyrrolidone) (PVP, molecular weight 1300 000), isopropanol (98%), potassium hydroxide (KOH  $\geq$  85%) and 5 wt% NAFION solution were purchased from Sigma-Aldrich.

## **2.2.Preparation of nanofibers**

In a typical procedure, 0.5 g of nickel acetate tetrahydrate and 0.0477 g of gadolinium nitrate hexahydrate were dissolved in a solvent mixture of 2mL DMF and 2 mL ethanol with overnight stirring (precursor solution) to obtain the Ni:Gd = 2.009:0.106 mole ratio. 0.5 g of PVP dispersed in 4 mL ethanol by stirring overnight was then added to the precursor solution. Nanofibers were spun in a home-built electrospinning apparatus at an electric potential of 25 kV with a feed rate of 2mL/ h from the obtained solution. Nanofibers were picked on a rotating coil covered with an aluminium foil with a rotation speed of 400 rpm for 15 cm from the syringe tip. The composite nanofibers were collected and calcined in a muffle furnace at 600 °C, with a heating rate of 1 °C/min, for 3 h under air or Ar atmosphere. In the following, the prepared nanofibers without Gd<sub>2</sub>O<sub>3</sub> are labelled as NiO, while the doped NiO nanofibers with 5 at% Gd then it has been calcined in different gases; air and Ar are denoted as Gd<sub>2</sub>O<sub>3</sub>/NiO and Ni/Gd<sub>2</sub>O<sub>3</sub>/NiO, respectively.

## **2.3.Characterization of nanofibers**

The phase composition of the materials was analyzed by X-ray diffraction (XRD), using a PANalytical Xpert-PRO diffractometer equipped with an Xcelerator detector using Ni-filtered Cu radiation (CuK $\alpha$ 1 radiation wavelength 0.1540598 nm and CuK $\alpha$ 2 radiation wavelength 0.1544426 nm) at 40 kV and 40 mA. In order to obtain XRD patterns with good quality, the nanofibers were well ground, and the obtained powder samples were scanned at a scanning rate of 0.1° min<sup>-1</sup> (i.e., step size and time of 0.02° and 12 seconds, respectively) in the 2 $\theta$  range of 10–90°. Rietveld refinement was performed using the FULLPROF program [56] with profile function 7 (Thompson-Cox-Hastings pseudo-Voigt convoluted with an axial divergence asymmetry function) [57]. The resolution function of the instrument was obtained from the structure refinement of a silicon standard. Raman spectra were measured on a Horiba XploRA using a diode lasers by Cobolt laser ( $\lambda$ = 638 nm) at a power of 10 mW and an objective microscope lens of 100x.

The morphology and structure of the obtained nanofibers were observed by scanning electron microscopy (SEM) (Hitachi S4800, Japan). Energy-dispersive X-ray spectroscopy analysis (EDX) with elemental mapping was performed with a Zeiss EVO HD15 microscope coupled to an Oxford X-MaxN EDX detector. The fiber morphology was examined also using high-resolution transmission electron microscopy (HRTEM, JEOL JEM 2100, Japan) equipped with energy-dispersive X-ray (EDX) spectroscopy. X-ray photoelectron spectroscopy (XPS) was performed using an Escalab 250 (Thermo Fisher Scientific, USA) using monochromatic Al K $\alpha$  (1486.6 eV) radiation at 2kV and 1  $\mu$ A. The surface diameter of 400  $\mu$ m was analyzed during the acquisition time of 1203.5 s for obtaining the elemental composition. Room-temperature continuous-wave (cw) electron paramagnetic resonance (EPR) measurements at X-band frequencies (9.78 GHz) were conducted with a Bruker B-ER420 spectrometer upgraded with a Bruker ECS 041XG microwave bridge and a lock-in amplifier (Bruker ER023M) using a Bruker TE102 resonator applying a modulation amplitude of 5 G and a modulation frequency of 100 kHz. The samples were measured in quartz tubes of 2.9 mm outer diameter. The elemental concentration in the nanofibers was detected using atomic absorption spectroscopy (AAS) (AAAnalyst 400, PerkinElmer). About 0.2 g of each nanofibers was annealed at 600 °C under air atmosphere for 6 h, and the obtained ash was dissolved in 2 mL of concentrated HNO<sub>3</sub> for 24 hrs. Then, the obtained solution was diluted in 0.2 L of water and used to detect Ni and Gd concentration by AAS.

## 2.4 Electrochemical measurements

The electrochemical tests were carried out by a Solartron SI 1287 galvanostatic-potentiostat in a three-electrode configuration with a platinum counter-electrode and a Ag/AgCl reference electrode (0.197 V vs. RHE at room temperature) in the presence of NAFION membrane (proton exchange membrane) to separate between the anode and cathode. During this measurement, 5 mg of prepared nanofibers were mixed with 1 mL of isopropanol and 40  $\mu$ l of NAFION solution by at least 15 min ultrasonication to form a homogeneous catalyst ink. Afterwards, 20  $\mu$ l of the ink was drop-casted on to a glassy carbon electrode of 3 mm diameter, dried and used as a working electrode. A Pt wire (CH-instrument, USA) was used on the cathode side as a standard material for comparison. The linear sweep voltammetry (LSV) curves were collected for HER at a potential scan rate of 5mV/s. The cyclic voltammograms (CV) were recorded in the potential range of 0.1 V to 0.3 V at a several scan rate of 10:100 mV/s. All electrochemical experiments were carried out at room temperature

and at ambient pressure in 1 M KOH as an electrolyte. The electrochemical impedance spectroscopy (EIS) was performed at 0.2 V vs. RHE in a frequency range of 0.1Hz to 1MHz with a voltage bias of 10 mV amplitude. Hydrogen measurements were recorded using gas chromatography (GC; Clarus-400, Perkin Elmer, TCD 2m\*1mm and He as carrier gas).

### 3. Results and discussion

The NiO, Gd<sub>2</sub>O<sub>3</sub>/NiO, and Ni/Gd<sub>2</sub>O<sub>3</sub>/NiO NFs were fabricated via electrospinning of polymeric solution containing nickel acetate and gadolinium nitrate as precursors. The XRD patterns of prepared NiO, Gd<sub>2</sub>O<sub>3</sub>/NiO and Ni/Gd<sub>2</sub>O<sub>3</sub>/NiO nanofibers were illustrated in Fig. 1. All XRD reflections observed in the pattern of NiO nanofiber can be assigned to the cubic NiO phase (space group *Fm-3m*, JCPDS card no. 01-75-0269) [58]. No additional reflections are observed, which could be attributed to impurities. we focussed on a narrower 2 $\Theta$  window for closer analysis in Fig 1b. By careful comparison of the observed peaks for each phase with those calculated from the respective reference structures of NiO (PDF #047-1049), Gd<sub>2</sub>O<sub>3</sub> (PDF #012-0797) and metallic Ni (PDF #004-0850), we can clearly see the peaks corresponding to the (222), (400) and (440) planes of Gd<sub>2</sub>O<sub>3</sub> phase at 2 $\theta$  of 28.6°, 33.14° and 47.57° and the (111) and (200) planes of NiO phase at 37.29° and 43.32°, as well as the (111) and (200) planes of Ni phase at 44.53° and 51.89°. Rietveld refinement of the XRD pattern of NiO nanofibers revealed that the sample is composed of nanocrystallites with a mean size of 27.3±0.7 nm and with a small microstrain of 1.63 x 10<sup>-4</sup>. The lattice parameter *a* of NiO phase in this sample was found to be 4.1762(2) Å, which is in good agreement with a previously reported value [58]. On the other hand, the NiO phase in the Gd<sub>2</sub>O<sub>3</sub>/NiO sample doped with 5 at% of Gd and calcined in air showed a slight increase in the lattice parameter in comparison with that of pure NiO nanofiber. This increase in the lattice parameter can be explained the substitution of larger Gd<sup>3+</sup> for smaller Ni<sup>2+</sup> cations in the NiO lattice [*r* (Gd<sup>3+</sup>) = 93.8 pm, *r* (Ni<sup>2+</sup>) = 69 pm; both ions are 6-fold coordinated [59]. A very small amount of nanocrystalline Gd<sub>2</sub>O<sub>3</sub> (1.4(4) wt%) is observed as a side phase, suggesting that the fraction of Gd<sup>3+</sup> in the NiO lattice is less than 5 at%. The calcination of the Ni/Gd<sub>2</sub>O<sub>3</sub>/NiO sample doped with 5 at% of Gd in argon atmosphere led to an increase in the amount of Gd<sub>2</sub>O<sub>3</sub> phase combined with the segregation of 2.3(3) wt% of metallic Ni. It has been reported that transition elements can be reduced during the thermal decomposition of organic carbon based-materials such as acetate or PVP materials in Ar atmosphere [60, 61]. Moreover, the lattice parameter of NiO

phase in this sample is quite similar to that of pure NiO nanofiber, confirming the segregation of  $\text{Gd}_2\text{O}_3$  from the NiO lattice during the calcination in Ar atmosphere. The lattice parameters of NiO, weight fractions, crystallite size, and microstructure of all samples as obtained by Rietveld refinement are listed in Table 1. As shown in Table 1, the crystallite size of NiO phase decreases with the addition of Gd dopant, which is consistent with the decrease in the size of NiO fibers as revealed by SEM characterizations (Fig. 2). The lower microstrain of NiO phase in the Ni/ $\text{Gd}_2\text{O}_3$ /NiO sample in comparison with that in  $\text{Gd}_2\text{O}_3$ /NiO sample is due to the segregation of  $\text{Gd}^{3+}$  and  $\text{Ni}^{2+}$  from NiO lattice by calcination in Ar atmosphere.

Raman scattering is a useful technique to study the defect and distortion of the crystalline lattices. The Raman spectra of the synthesized nanofibers are illustrated in Figure S1. The broad peak observed at  $510\text{ cm}^{-1}$  in the Raman spectra of all samples can be attributed to the Ni–O [53]. This peak is shifted to lower wavenumber for  $\text{Gd}_2\text{O}_3$ /NiO nanofibers if compared with those of the other two samples. This shift can be explained by the increase in the unit cell volume of NiO phase in  $\text{Gd}_2\text{O}_3$ /NiO nanofibers due to the substitution of  $\text{Ni}^{2+}$  by  $\text{Gd}^{3+}$ , as confirmed by XRD characterizations. The increase in cell volume is accompanied by an increase in the bond distances, thus, a decrease in the force constant and the corresponding wavenumber [62]. Moreover, the peak observed at  $\sim 355\text{ cm}^{-1}$  in the Raman spectrum of Ni/ $\text{Gd}_2\text{O}_3$ /NiO sample can be assigned to the  $\text{Gd}_2\text{O}_3$  phase [63]. These results are in good agreement with XRD results [63].

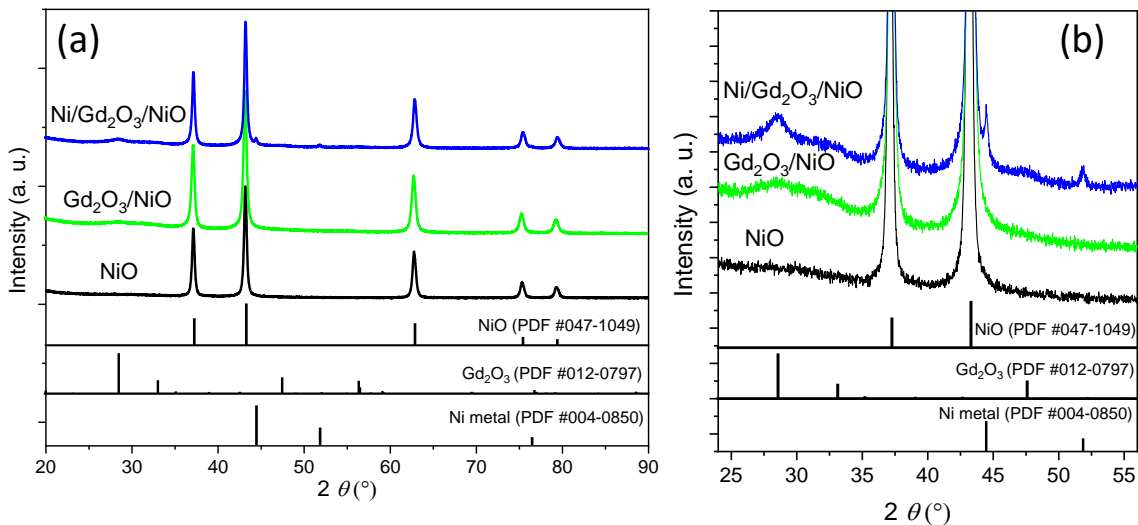


Fig. 1: XRD patterns of prepared NiO,  $\text{Gd}_2\text{O}_3$ /NiO, and Ni/ $\text{Gd}_2\text{O}_3$ /NiO nanofibers. Panels b focusses on a narrower  $2\Theta$  window for closer analysis. The lower panel indicates the phase

assignment to the respective reference structures of NiO (PDF #047-1049), Gd<sub>2</sub>O<sub>3</sub> (PDF #012-0797) and metallic Ni (PDF #004-0850).

**Table 1:** Summary of structural parameters extracted from powder XRD patterns by Rietveld refinement of NiO, Gd<sub>2</sub>O<sub>3</sub>/NiO, and Ni/Gd<sub>2</sub>O<sub>3</sub>/NiO nanofibers.

Sample	NiO phase				Gd <sub>2</sub> O <sub>3</sub>		Ni metal	
	Lattice parameter (Å)	Weight fraction (%)	Crys. size (nm)	Microstrain x 10 <sup>-4</sup>	Weight fraction (%)	Crys. size (nm)	Weight fraction (%)	Crys. size (nm)
NiO	4.1762(2)	100	27.3(8)	1.63	-	-	-	-
Gd <sub>2</sub> O <sub>3</sub> /NiO	4.1767(2)	98.6(6)	18.7(5)	1.56	1.4(4)	2.9(1)	-	-
Ni/Gd <sub>2</sub> O <sub>3</sub> /NiO	4.1760(1)	94.4(6)	22.4(7)	1.12	3.3(2)	4.2(1)	2.3(3)	26.6(8)

The differences between the morphology of the three prepared fibers are illustrated by the scanning electron microscopy images presented in Fig. 2(a-c). The NiO fibers are large (a few hundred nanometers width) and randomly distributed with a web-like morphology, and they are constituted of NiO individual particles. This could be explained by the bending instabilities and the partial evaporation of solvents, which were linked through hydrogen bonding [64-66]. The Gd<sub>2</sub>O<sub>3</sub>/NiO and Ni/Gd<sub>2</sub>O<sub>3</sub>/NiO samples exhibit thinner (less than 100 nanometers) and longer fibers than NiO sample due to the doping with Gd. The contrast is highly regular inside the fibers for Gd<sub>2</sub>O<sub>3</sub>/NiO, whereas particles like globules appear in addition for Ni/Gd<sub>2</sub>O<sub>3</sub>/NiO. These observations are confirmed by the HRTEM investigations. NiO NFs are mainly composed of large spherical and quasi-spherical nanoparticles (Fig. S2). These NiO nanoparticles are highly crystalline in nature as revealed by the well-resolved lattice fringes of HRTEM image and the fast Fourier transform (FFT) pattern (Fig. S3 (a)). Average fringe distances of 2.05±0.05 and 2.36±0.05 Å corresponding to the (200) and (111) planes distances in NiO phase, respectively, are observed in the HRTEM image of Gd<sub>2</sub>O<sub>3</sub>/NiO sample (Fig. 2d). The FFT pattern Gd<sub>2</sub>O<sub>3</sub>/NiO sample (Fig. S3b) reveals the lattice spacings related to the (111), (200) and (220) planes of NiO as well as the (220) and (331) planes (*d* spacings of 0.19 nm and 0.12 nm, respectively) of Gd<sub>2</sub>O<sub>3</sub>. These results are in good agreement with XRD results, which reveals the presence of crystalline NiO and Gd<sub>2</sub>O<sub>3</sub> in

Gd<sub>2</sub>O<sub>3</sub>/NiO sample. Moreover, EDX elemental mapping shows that the Gd, O, and Ni elements were uniformly distributed in Gd<sub>2</sub>O<sub>3</sub>/NiO nanofibers (Fig. 2e-h), confirming the incorporation of Gd into the NiO lattice. In contrast, Gd was mostly observed on the surface of NiO fibers in Ni/Gd<sub>2</sub>O<sub>3</sub>/NiO sample ((Fig. 2j-m)), which can be explained by the segregation of Gd<sub>2</sub>O<sub>3</sub> and metallic Ni phases after calcination in Ar atmosphere as coaxial nanofibers structure. The FFT pattern of Ni/Gd<sub>2</sub>O<sub>3</sub>/NiO (Fig. S3-c) confirms the formation of the cubic Ni metal ((111) plane correspond to *d* distance of 0.2 nm) in addition to NiO and Gd<sub>2</sub>O<sub>3</sub> phases. Moreover, FFT analysis shows that the spherical nanoparticles observed on the surface of the NiO fibers (Fig. 2c) are mainly metallic Ni. These results are in good agreement with those obtained from Rietveld refinement of XRD data (see Table 1). Moreover, AAS analysis demonstrated that Ni:Gd atomic ratio is about 2.008:0.053 in both Gd<sub>2</sub>O<sub>3</sub>/NiO and Ni/Gd<sub>2</sub>O<sub>3</sub>/NiO samples. The lower amount of Gd in the samples if compared with that used in the electrospinning experiments (i.e., Ni:Gd mole ratio = 2.009:0.106) suggests that not all Gd precursor has been successfully loaded on the NiO nanofibers. However, the similar content of Ni and Gd in both Gd<sub>2</sub>O<sub>3</sub>/NiO and Ni/Gd<sub>2</sub>O<sub>3</sub>/NiO nanofibers indicates that the two samples differ only in the structure and morphology.

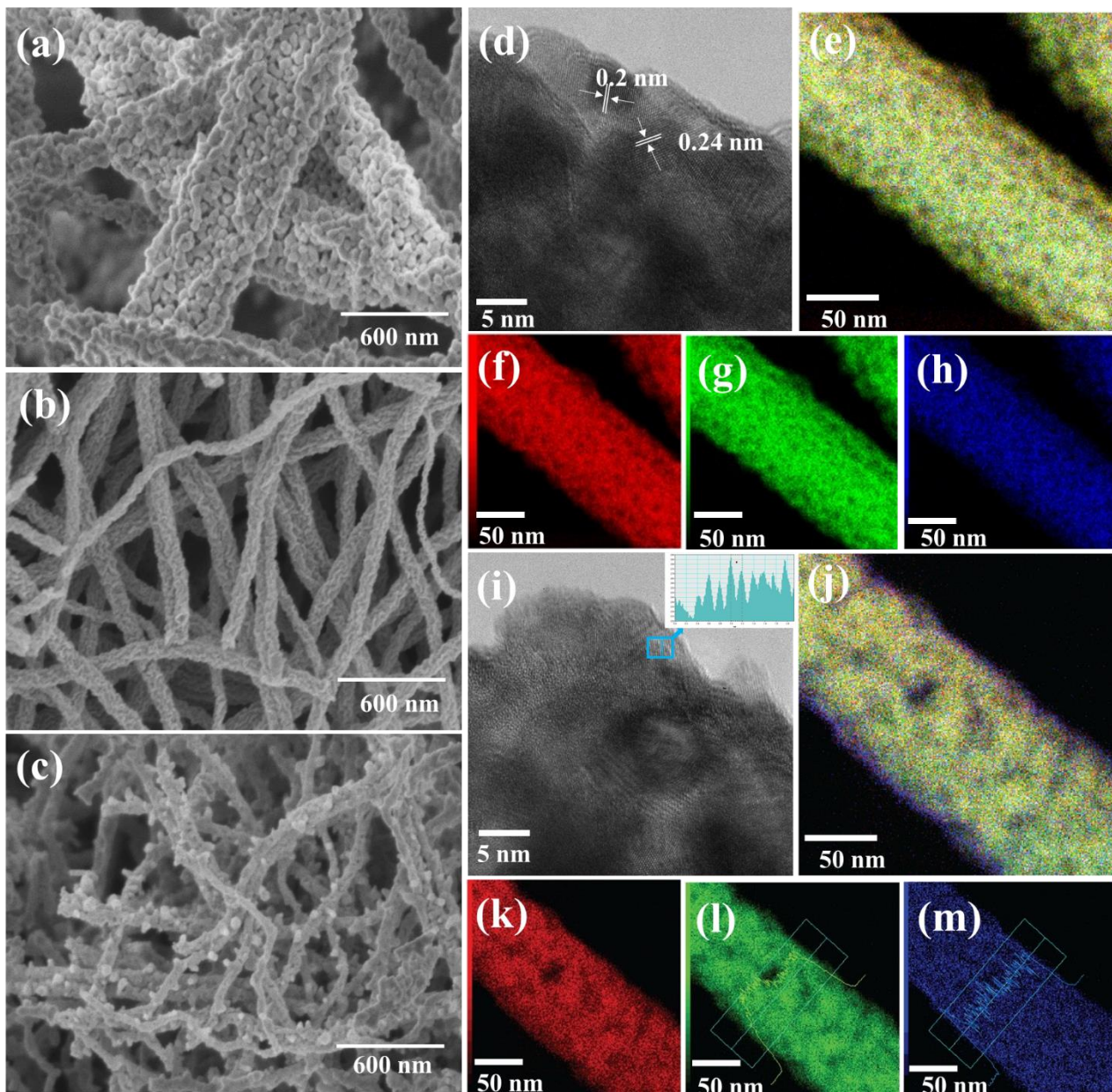


Fig. 2: Field emission SEM images of the prepared nanofibers; NiO (a), Gd<sub>2</sub>O<sub>3</sub>/NiO (b), and Ni/Gd<sub>2</sub>O<sub>3</sub>/NiO (c). High-resolution transition microscope (d and i) with EDX elemental mapping (e-h and j-m) of Gd<sub>2</sub>O<sub>3</sub>/NiO (d, e-h) and Ni/Gd<sub>2</sub>O<sub>3</sub>/NiO (i, j-m) and the fast Fourier transform (FFT) pattern of the area marked by the blue square box of Ni/Gd<sub>2</sub>O<sub>3</sub>/NiO and the corresponding intensity profiles in the inset (i), the oxygen (f and k), nickel (g and l) and gadolinium (h and m). The line-scans in (l) and (m) images confirm the segregation of gadolinium on the surface of nanofibers.

XPS measurements further revealed the elemental compositions, chemical bonding, and oxidation states of Ni, O, and Gd. As shown in Fig. S4, the survey XPS spectra of prepared NFs confirm the elemental composition of the obtained fibers and the presence of a small amount of carbon originated from organic acetate or PVP materials used in the synthesis. The high-resolution Ni 2p, Gd 4d and O 1s spectra are shown in Fig 3a-c. The Ni 2p<sub>3/2</sub> spectra (Fig. 3a) of NiO and Gd<sub>2</sub>O<sub>3</sub>/NiO nanofibers can be fitted with two peaks at 853.9 and 855.5 eV with a broad satellite peak at around 861.1 eV, in good agreement with the previous reports for NiO [67]. For Ni/Gd<sub>2</sub>O<sub>3</sub>/NiO, these XPS peaks are shifted to lower binding energy, suggesting a decrease of the oxidation state of nickel cations, in agreement with the observation of Ni metal by XRD (Fig. 1). The O 1s spectra (Fig. 3b) can be deconvoluted into three peaks around 529, 531 and 532 eV corresponding to the oxygen lattice O<sup>2-</sup>, hydroxides and adsorbed oxygen (i.e. adsorbed H<sub>2</sub>O), respectively [50]. For the Ni/Gd<sub>2</sub>O<sub>3</sub>/NiO sample, the peak corresponding to the lattice oxygen is shifted to lower binding energy, which can be explained by a decrease of the oxygen content in this sample in connection with the reducing conditions of the annealing. Moreover, a high amount of hydroxides is observed on the surface of Ni/Gd<sub>2</sub>O<sub>3</sub>/NiO sample calcined in Ar. The Gd 3d spectra of Gd<sub>2</sub>O<sub>3</sub>/NiO and Ni/Gd<sub>2</sub>O<sub>3</sub>/NiO (Fig 3c) can be fitted with one peak located at 1189 eV assigned to Gd 3d<sub>5/2</sub> of Gd<sub>2</sub>O<sub>3</sub> [68].

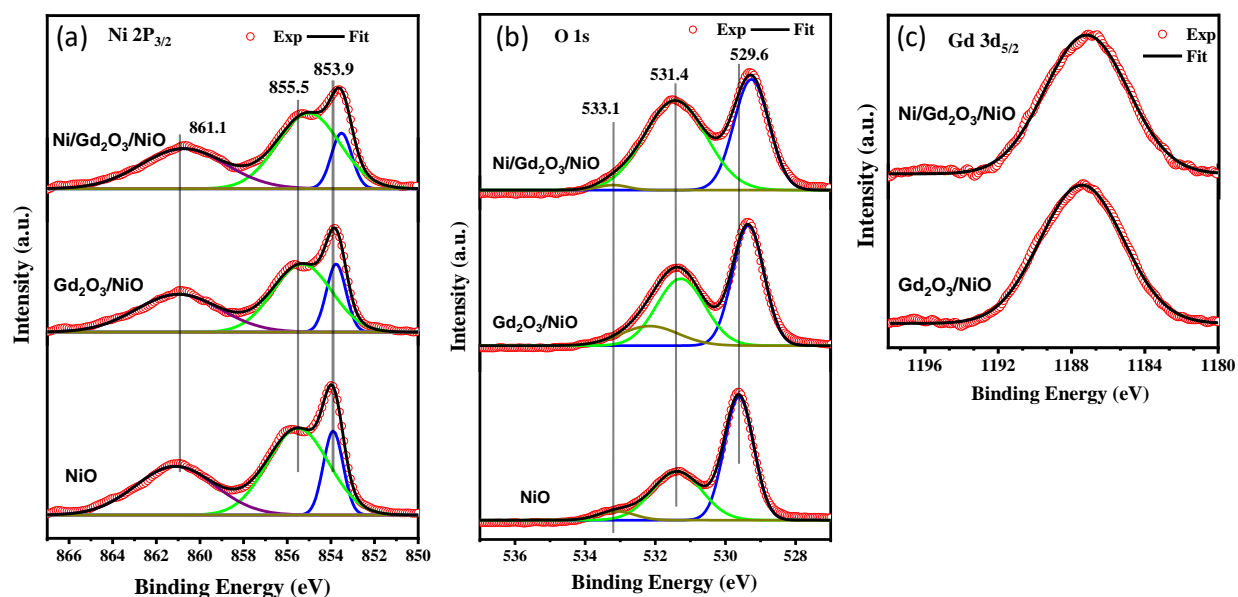


Fig. 3: High-resolution XPS spectra of Ni 2p (a), O 1s (b), and Gd 3d (c) for NiO, Gd<sub>2</sub>O<sub>3</sub>/NiO, and Ni/Gd<sub>2</sub>O<sub>3</sub>/NiO nanofibers.

Fig. 4 shows the room temperature continuous-wave (cw) EPR spectra of NiO, Gd<sub>2</sub>O<sub>3</sub>/NiO, and Ni/Gd<sub>2</sub>O<sub>3</sub>/NiO samples. The spectra were normalized to sample mass. For all samples, the EPR spectra show a broad line around  $g \approx 2.3$  with the intensity and  $\Delta B_{pp}$  linewidth varying in a complex way for the different samples. The observed  $g$ -values are within the range of  $g$ -values previously reported for NiO particles [69, 70]. For the Gd<sub>2</sub>O<sub>3</sub>/NiO sample, a clear decrease in EPR intensity can be detected compared to NiO sample, supporting the assumption that mainly Ni species contribute to the detected signal. The intensity decrease is qualitatively comparable to previous results on Gd-doped NiFe<sub>2</sub>O<sub>4</sub>, as reported by Dixit *et al.* [71]. It is perceivable that Gd<sup>3+</sup> ions replace Ni-ions lowering, thereby the signal intensity attributed to Ni-ions. The EPR spectra with a dominant broad signal centered around  $g \approx 2.3$  did not allow for a clear identification of Gd<sup>3+</sup> related signals expected at  $g$ -values  $\leq 2.05$  [72]. The  $\Delta B_{pp}$  linewidth is slightly higher for Gd<sub>2</sub>O<sub>3</sub>/NiO compared to NiO despite the decrease in intensity indicative for significant  $g$ -value broadening evidenced for both samples in 34 GHz measurements (data not shown). The Ni/Gd<sub>2</sub>O<sub>3</sub>/NiO sample exhibits the highest EPR intensity and  $\Delta B_{pp}$  linewidth suggesting the highest number of EPR-active species within the sample series. There are several possible origins for this intensity enhancement: Compared to Gd<sub>2</sub>O<sub>3</sub>/NiO, the number of replaced Ni ions is expected to be decreased, as increased Gd<sub>2</sub>O<sub>3</sub> segregation is evidenced by XRD. Additionally, the fibers size and defect density may affect the signal, as EPR detects only a part of the Ni species in NiO exhibiting in bulk antiferromagnetic ordering ( $T_{N\acute{e}el} = 250$  °C) [70, 73]. Moreover, as segregation of Ni metal is revealed by XRD analysis, metallic Ni nanoparticles ( $g \approx 2.25$  depending on the distance between particles) [74-76] may contribute to the observed signal.

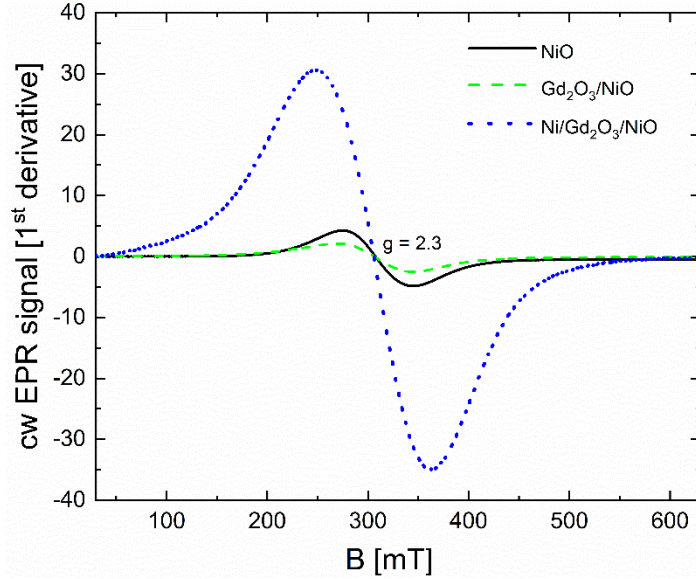


Fig. 4: Room temperature cw EPR spectra of NiO, Gd<sub>2</sub>O<sub>3</sub>/NiO, and Ni/Gd<sub>2</sub>O<sub>3</sub>/NiO nanofibers (9.78 GHz, 5 G, 100 kHz, 2 mW mw power). Spectra are normalized to sample mass.

The mechanism of formation of Ni/Gd<sub>2</sub>O<sub>3</sub>/NiO heterostructure during calcination in argon atmosphere can be explained as follows. During calcining the electrospun nanofibers in air or oxygen atmosphere, many oxygen vacancies are usually expected to be generated in the NiO lattice, while on cooling, the atmospheric oxygens fill these oxygen vacancies in the NiO nanofibers again. In contrast, during calcining the nanofibers in oxygen-free atmosphere (e.g. argon), there are no sufficient oxygens to fill back the generated oxygen vacancies on the surface of the nanofibers. In consequence, Gd<sub>2</sub>O<sub>3</sub> is segregated to the surface as well as a partial reduction of NiO into metallic Ni is taken place as the charge compensation. Therefore, the Ni/Gd<sub>2</sub>O<sub>3</sub>/NiO heterostructure is formed only while performing the calcination of the nanofibers in argon atmosphere. Our finding is consistent with previous works showed the formation of similar Ni/NiO heterostructure by calcining electrospun Ni-organic nanofibers in argon atmosphere [49].

The electrocatalytic activities of NiO, Gd<sub>2</sub>O<sub>3</sub>/NiO and Ni/Gd<sub>2</sub>O<sub>3</sub>/NiO for HER were investigated, and commercial Pt tested for comparison (Fig 5). The LSV curve in Fig.5a revealed that the NiO sample shows poor performance for HER. In contrast, Gd<sub>2</sub>O<sub>3</sub>/NiO exhibits good HER activity due to the substitution of Ni<sup>2+</sup> with Gd<sup>3+</sup> in the NiO lattice as confirmed in the previous section on the sample characterization. The presence of Gd<sub>2</sub>O<sub>3</sub> as impurity could be another reason for the good

electrocatalytic activity of this sample, since such an enhancement of the electrocatalytic activity is achieved by adding Gd/Gd<sub>2</sub>O<sub>3</sub> particles in Ni-Co and Ni-CeO<sub>2</sub>-Gd electrodes to HER [51, 52]. The highest HER activity is observed for Ni/Gd<sub>2</sub>O<sub>3</sub>/NiO, requiring only a small overpotential of 190 mV to achieve a current density of 10 mA/ cm<sup>2</sup>. However, the activity is as still slightly lower than that of a Pt plate (160 mV@10 mA/ cm<sup>2</sup>), whereas the onset potential of Ni/Gd<sub>2</sub>O<sub>3</sub>/NiO is lower than that of Pt, which recommended it for potential industrial application in HER. The high activity of Ni/Gd<sub>2</sub>O<sub>3</sub>/NiO sample can be explained by four reasons: (i) the segregation of Gd<sub>2</sub>O<sub>3</sub> on the surface of NiO fibers, (ii) formation of active Ni metal via the reduction in Ar atmosphere, (iii) the smaller fiber diameter and (iv) high amount of OH<sup>-</sup> on the surface of the fibers.

Tafel slopes are given by fitting the linear regions of Tafel plots to the Tafel equation ( $\eta = b \log |j| + a$ , where  $b$  is the Tafel slope and  $j$  the current density). As demonstrated in Fig. 5c, the Tafel slope value of Ni/Gd<sub>2</sub>O<sub>3</sub>/NiO nanofibers (45 mV/dec) is smaller than those of NiO (120 mV/dec), and Gd<sub>2</sub>O<sub>3</sub>/NiO (53 mV/dec) but larger than that of Pt (30 mV/dec). The current exchange densities ( $j_0$ ) of prepared samples are estimated from the Tafel plots via extrapolation. The values of  $j_0$  for NiO, Gd<sub>2</sub>O<sub>3</sub>/NiO and Ni/Gd<sub>2</sub>O<sub>3</sub>/NiO nanofibers were gathered in Table 2, confirming the superior performance of Ni/Gd<sub>2</sub>O<sub>3</sub>/NiO. Ni<sup>0</sup> has a convenient H atom binding energy close to Pt [77, 78]. Whither, Ni<sup>0</sup> on the surface of Ni/Gd<sub>2</sub>O<sub>3</sub>/NiO nanofibers would facilitate H adsorption and thus the Volmer process. The roles of segregated Gd<sub>2</sub>O<sub>3</sub> on the surface of Ni/Gd<sub>2</sub>O<sub>3</sub>/NiO could accelerate both Volmer and Heyrovsky processes and reduce the resistance to drive HER with higher exchange current density at low overpotentials via liberations of additional reactive sites. Wheresoever, the OH<sup>-</sup> generated by H<sub>2</sub>O splitting could preferentially attach to a Gd<sub>2</sub>O<sub>3</sub> site at the interface due to strong electrostatic affinity to the locally positively charged Gd<sup>3+</sup> species and more unfilled 5d orbitals. Furthermore, the segregation of Gd<sub>2</sub>O<sub>3</sub> to Ni-based materials could increase their corrosion resistance and stability [54]. Additionally, the voltammetric study of NFs within the potential range of +0.1 to +0.3 V, where no faradic reaction occurred (Fig. S5), is used to calculate the double-layer capacitance ( $C_{dl}$ ) of NFs as illustrated in Fig. 5d and summarized in Table 2. The  $C_{dl}$  is linearly proportional to the effective electrochemical active surface area (EEASA). Electrochemically active surface area (ECSA) was evaluated from the following equation;  $ECSA = C_{dl}/C_s$ , where  $C_{dl}$  is the electrochemical double-layer capacitance and  $C_s = 40 \mu\text{F}/\text{cm}^2$ , is the capacitance of an atomically smooth planar surface [79]. Ni/Gd<sub>2</sub>O<sub>3</sub>/NiO catalyst has a  $C_{dl}$  value 1.2 and 6.6 times higher than Gd<sub>2</sub>O<sub>3</sub>/NiO and NiO, respectively. The tests mark

that more active sites are available for Ni/Gd<sub>2</sub>O<sub>3</sub>/NiO catalysts. Long-term durability for HER is of great significance for industrial applications. The chronoamperometric response for 60h (Fig. 5e) shows a slight current attenuation of 5% after 60h of continuous testing [80]. Likewise, the working electrode was submitted to 5000 cycles of a continuous cyclic voltammetry measurement between 0 and -0.3V (vs. RHE). As demonstrated in Fig. 5f, the LSV curves before and after 5000 CV test closely overlap, especially in the low overpotential region. The SEM image of the prepared Ni/Gd<sub>2</sub>O<sub>3</sub>/NiO nanofibers after the 60h electrolysis test in Fig. S6 was revealed that the morphology remains unaltered. We can also note that the crystallinity of Ni/Gd<sub>2</sub>O<sub>3</sub>/NiO nanofibers (Fig. S7) was stable after 60h as confirmed by XRD. These results confirm that the Ni/Gd<sub>2</sub>O<sub>3</sub>/NiO catalyst possesses superior stability in the long term HER process compared to the previously reported NiO system (Table S1) [3, 48-53, 81].

Moreover, the faradic efficiency of Ni/Gd<sub>2</sub>O<sub>3</sub>/NiO of about 98 % was determined by GC measurements of evolved H<sub>2</sub>, as shown in Fig. 5g. In addition, the highest faradic efficiency could be attributed to the enrichment of electron transfer in Ni/Gd<sub>2</sub>O<sub>3</sub>/NiO as seen from EIS measurements of Fig. 5h. To determine the internal resistance and charge transport of the prepared nanofibers, electrochemical impedance spectroscopy measurements were performed. Fig. 5h shows the Nyquist plot of the prepared NiO, Gd<sub>2</sub>O<sub>3</sub>/NiO, and Ni/Gd<sub>2</sub>O<sub>3</sub>/NiO nanofibers in the frequency range of 100 kHz to 0.1 Hz with a signal amplitude of 10 mV. The EIS plot can be easily distinguished into a small semicircle at the high-frequency region, which identified with Randles cell and a straight line with a slope towards the low-frequency region where semi-infinite diffusion is the rate-determining step with Warburg impedance. The semicircle represents the charge transfer process, and the sloped line represents the capacitance of the double layer of the nanofibers with Warburg impedance. The equivalent series resistance (ESR) could be estimated from the intercept at the real impedance axis; it was found to be around 0.6 Ω, which constitutes the electrolyte resistance, the resistance at electrode-electrolyte interface and the electrode material internal resistance. The semicircle diameter value reveals the charge transfer resistance (R<sub>ct</sub>), as illustrated in Table 2. The impedance spectrum was subjected to the Randles equivalent circuit with mixed kinetic and charge transfer control, as shown in the inset of Fig. 5h, which consists of bulk solution resistance (R<sub>s</sub>), charge transfer resistance (R<sub>ct</sub>), Warburg impedance related to the electrolyte ion diffusion (Z<sub>w</sub>) and double-layer capacitance (C<sub>dl</sub>). The lower value of R<sub>ct</sub> was attributed to the high interfacial conductivity of Ni nanoparticles on the surface of NFs of Ni/Gd<sub>2</sub>O<sub>3</sub>/NiO and its

large slope in the low-frequency region of the Nyquist plot was ascribed to the Warburg behaviour, which arises from the fast ion diffusion across the electrode-electrolyte interface.

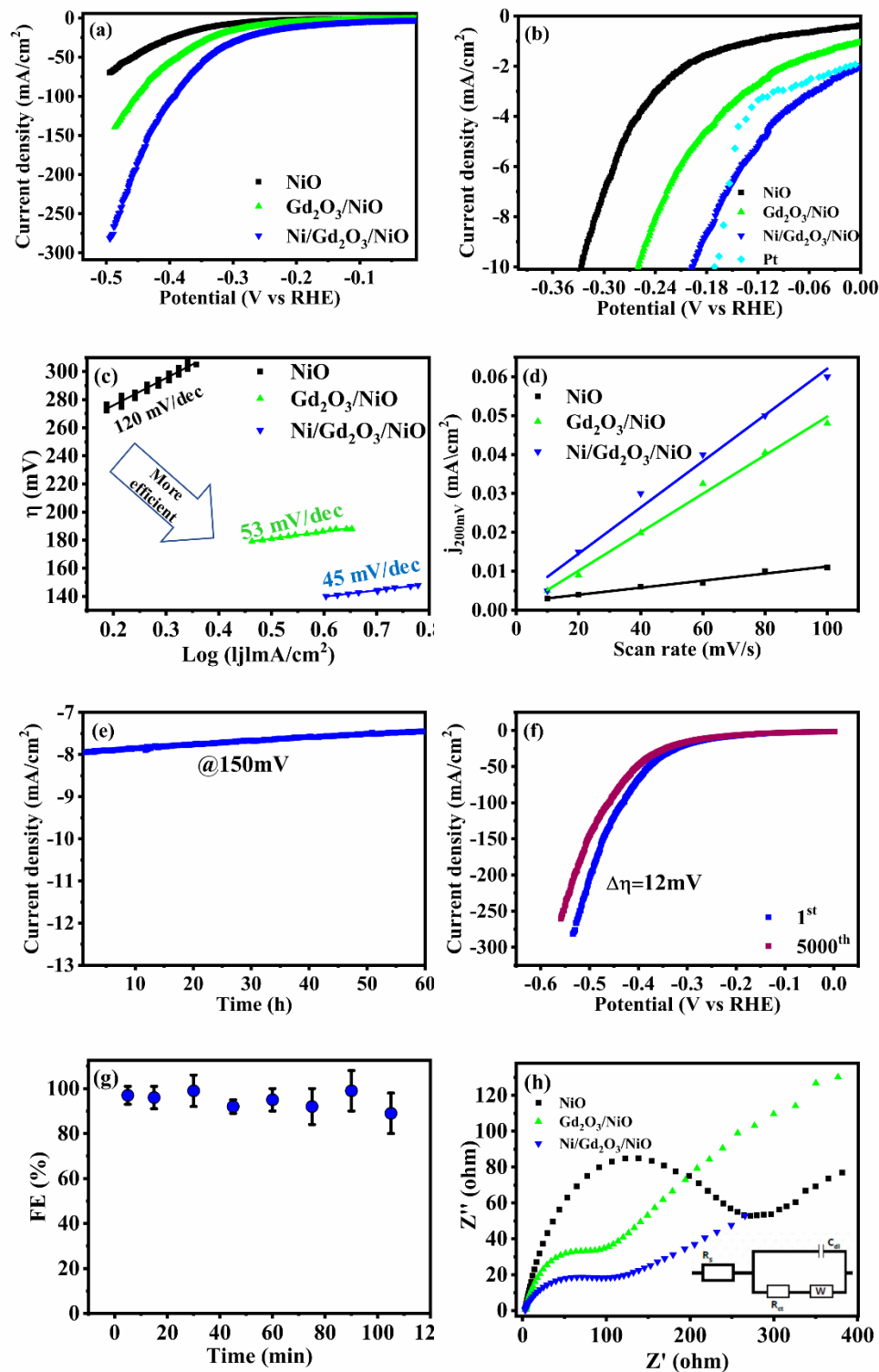


Fig. 5: a) LSV curves of NiO, Gd<sub>2</sub>O<sub>3</sub>/NiO and Ni/Gd<sub>2</sub>O<sub>3</sub>/NiO NFs for HER at 5mV/s in 1M KOH, b) LSV curves at 10 mA/cm<sup>2</sup> of the NFs and commercial Pt at 5mV/s in 1M KOH, c) Tafel plots of prepared NFs, d) estimation of C<sub>dl</sub> through plotting the current density variation ( $\Delta j = (j_a - j_c)/2$ ), at 200 mV vs. RHE; data obtained from the CV in Fig.S2) against scan rate to fit a linear regression, e) chronoamperometry test of Ni/Gd<sub>2</sub>O<sub>3</sub>/NiO at 150 mV, f) LV curves before and after 5000CV test of Ni/Gd<sub>2</sub>O<sub>3</sub>/NiO electrode at 5mV/s in 1M KOH, g) Faradic Efficiency of Ni/Gd<sub>2</sub>O<sub>3</sub>/NiO at 350 mV vs. RHE for HER in 1M KOH saturated with Ar for 30 min before the experiment, the concentration of evolved H<sub>2</sub> was quantified every 15 min and h) EIS Nyquist plots in a frequency range of 0.1Hz to 1MHz of NFs with equivalent circuit proposed in the inset.

### HER reaction mechanism

The Tafel slope was revealed the mechanism and kinetics of the HER reaction. HER mechanism in alkaline media follows either the Volmer – Heyrovsky or Volmer – Tafel reaction. A Tafel slope (b) of 120, 40 or 30 mV/dec should be obtained when the Volmer, Heyrovsky or Tafel reaction is rate-determining step (RDS), respectively.

- Volmer reaction is electroreduction of water molecules with electrons on the active sites of the cathode ( $* + \text{H}_2\text{O} + \text{e}^- \rightarrow * \text{H}_{\text{ads}} + \text{OH}^-$ ),
- Heyrovsky reaction is electrochemical hydrogen desorption ( $* \text{H}_{\text{ads}} + \text{H}_2\text{O} + \text{e}^- \rightarrow \text{H}_2 \uparrow + \text{OH}^-$ ),
- Tafel reaction is chemical desorption ( $2\text{H}_{\text{ads}} \leftrightarrow \text{H}_2 \uparrow$ ).

As illustrated in Fig. 6, the HER at Ni/Gd<sub>2</sub>O<sub>3</sub>/NiO NFs surface with b = 45 mV/dec follows a Volmer-Heyrovsky mechanism, and the RDS is determined by electrochemical desorption (H<sub>2</sub>O discharge and desorption of H<sub>2</sub> from the catalyst surface).

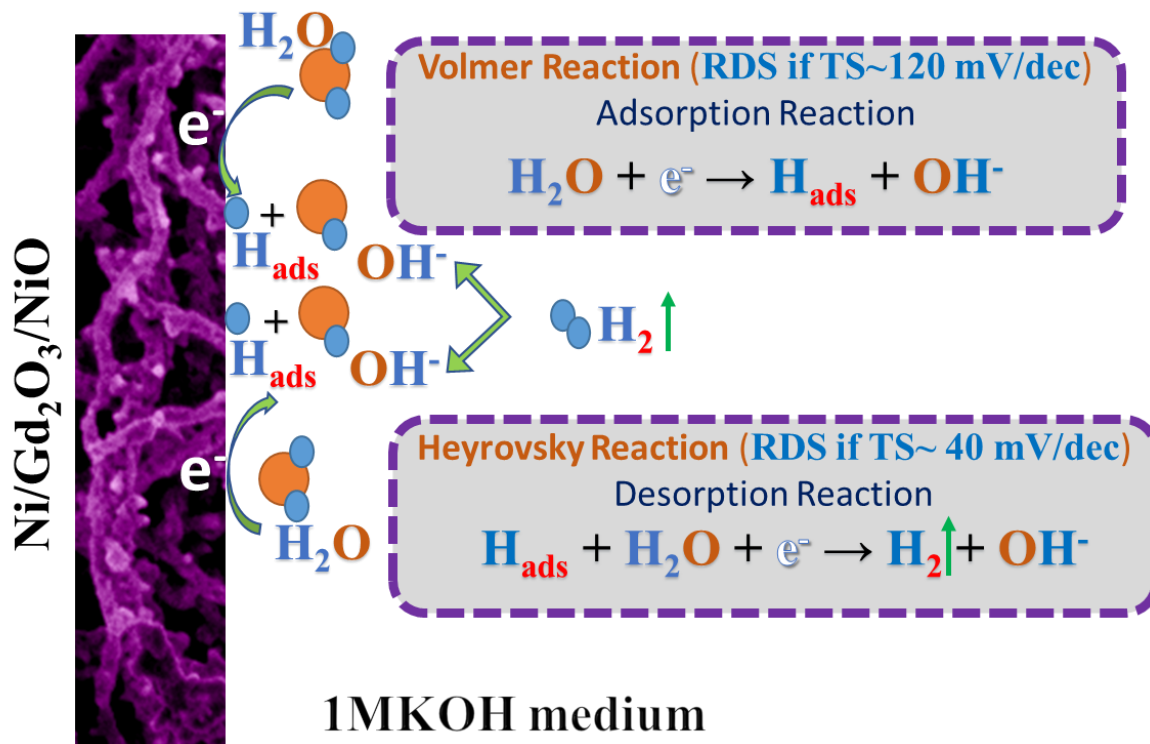


Fig. 6: Mechanism of HER on the surface of Ni/Gd<sub>2</sub>O<sub>3</sub>/NiO NFs.

**Table 2:** A summary of the electrochemical data of NiO, Gd<sub>2</sub>O<sub>3</sub>/NiO, and Ni/Gd<sub>2</sub>O<sub>3</sub>/NiO nanofibers for HER.

NFs	$\eta_{10}$ (mV)	$\eta_{\text{onset}}$ (mV)	$\text{TS}_{\text{HER}}$ (mV/dec)	Cdl ( $\mu\text{F}/\text{cm}^2$ )	ECSA ( $\text{cm}^2$ )	$j_0$ ( $\text{mA}/\text{cm}^2$ )	$R_s$ ( $\Omega$ )	$R_{\text{ct}}$ ( $\Omega$ )
NiO	326	233	120	90	2.24	1.21	3.2	349
Gd <sub>2</sub> O <sub>3</sub> /NiO	230	139	53	495	12.37	1.64	3.5	114
Ni/Gd <sub>2</sub> O <sub>3</sub> /NiO	190	89	45	594	14.85	1.85	3.1	93

$\eta_{10}$ : Overpotential at 10 mA/cm<sup>2</sup>,  $\eta_{\text{onset}}$ : Onset potential, TS: Tafel slope of HER,

### Conclusion

Simple and cost-effective NiO, Gd<sub>2</sub>O<sub>3</sub>/NiO and Ni/Gd<sub>2</sub>O<sub>3</sub>/NiO nanofibers prepared by electrospinning have been designed as superior HER electrocatalysts. In short, Ni/Gd<sub>2</sub>O<sub>3</sub>/NiO has the lowest one set potential ~ 32 mV, the smallest Tafel slope value 45 mV/dec and the highest exchange current density of 1.85 mA/cm<sup>2</sup>, i.e; characteristics comparable to most noble metal-free catalysis. This specific new catalyst design is promising for key renewable energy systems. Based

on experimental studies, we demonstrated that the chemical and electrical properties of NiO NFs are successfully optimized through Ni/Gd<sub>2</sub>O<sub>3</sub>/NiO heterostructures; the Gd ions doped on NiO NFs and the segregation of Gd<sub>2</sub>O<sub>3</sub> on the surface of NiO fibers remarkably enhance their electronic conduction and promote HER reaction kinetics simultaneously. Ni/Gd<sub>2</sub>O<sub>3</sub>/NiO offers the advantages of long-term durability after an accelerated scan of 5000 cycles as well as ready integration into an electrolyzes for HER, affording better performance than benchmark Pt catalysts.

## References

- [1] W. Yang, X. Yang, J. Jia, C. Hou, H. Gao, Y. Mao, C. Wang, J. Lin, X. Luo, Oxygen vacancies confined in ultrathin nickel oxide nanosheets for enhanced electrocatalytic methanol oxidation, *Applied Catalysis B: Environmental*, 244 (2019) 1096-1102.
- [2] M. Gong, W. Zhou, M.-C. Tsai, J. Zhou, M. Guan, M.-C. Lin, B. Zhang, Y. Hu, D.-Y. Wang, J. Yang, Nanoscale nickel oxide/nickel heterostructures for active hydrogen evolution electrocatalysis, *Nature communications*, 5 (2014) 1-6.
- [3] M. Chu, L. Wang, X. Li, M. Hou, N. Li, Y. Dong, X. Li, Z. Xie, Y. Lin, W. Cai, Carbon coated nickel-nickel oxide composites as a highly efficient catalyst for hydrogen evolution reaction in acid medium, *Electrochimica Acta*, 264 (2018) 284-291.
- [4] J.Y. Lee, K. Liang, K.H. An, Y.H. Lee, Nickel oxide/carbon nanotubes nanocomposite for electrochemical capacitance, *Synthetic metals*, 150 (2005) 153-157.
- [5] M.-S. Wu, Y.-A. Huang, C.-H. Yang, J.-J. Jow, Electrodeposition of nanoporous nickel oxide film for electrochemical capacitors, *International Journal of Hydrogen Energy*, 32 (2007) 4153-4159.
- [6] W.G. Nunes, L.M. Da Silva, R. Vicentini, B.G. Freitas, L.H. Costa, A.M. Pascon, H. Zanin, Nickel oxide nanoparticles supported onto oriented multi-walled carbon nanotube as electrodes for electrochemical capacitors, *Electrochimica Acta*, 298 (2019) 468-483.
- [7] N. Wang, H. Song, H. Ren, J. Chen, M. Yao, W. Huang, W. Hu, S. Komarneni, Partly nitrogenized nickel oxide hollow spheres with multiple compositions for remarkable electrochemical performance, *Chemical Engineering Journal*, 358 (2019) 531-539.
- [8] F. Tietz, F.J. Dias, D. Simwonis, D. Stöver, Evaluation of commercial nickel oxide powders for components in solid oxide fuel cells, *Journal of the European Ceramic Society*, 20 (2000) 1023-1034.
- [9] K.-H. Wang, H. Ikeuchi, T. Kawai, Enhanced Electrochromic Properties of a Nickel Oxide-Alanine Film, in: *Meeting Abstracts, The Electrochemical Society*, 2019, pp. 2269-2269.
- [10] Á. Balog, C. Janáky, The Effect of Trap States on the Optoelectronic Properties of Nanoporous Nickel Oxide, *Journal of The Electrochemical Society*, 166 (2019) H3265-H3270.
- [11] R. Newman, R. Chrenko, Optical properties of nickel oxide, *Physical Review*, 114 (1959) 1507.
- [12] W. Xing, F. Li, Z.-f. Yan, G. Lu, Synthesis and electrochemical properties of mesoporous nickel oxide, *Journal of Power Sources*, 134 (2004) 324-330.
- [13] K. Rao, A. Smakula, Dielectric properties of cobalt oxide, nickel oxide, and their mixed crystals, *Journal of Applied Physics*, 36 (1965) 2031-2038.
- [14] Y.-M. Lu, W.-S. Hwang, J. Yang, H. Chuang, Properties of nickel oxide thin films deposited by RF reactive magnetron sputtering, *Thin Solid Films*, 420 (2002) 54-61.

- [15] M.K. Carpenter, R.S. Conell, D.A. Corrigan, The electrochromic properties of hydrous nickel oxide, *Solar energy materials*, 16 (1987) 333-346.
- [16] Y.-z. Zheng, H.-y. Ding, M.-l. Zhang, Preparation and electrochemical properties of nickel oxide as a supercapacitor electrode material, *Materials Research Bulletin*, 44 (2009) 403-407.
- [17] M.-S. Wu, H.-H. Hsieh, Nickel oxide/hydroxide nanoplatelets synthesized by chemical precipitation for electrochemical capacitors, *Electrochimica Acta*, 53 (2008) 3427-3435.
- [18] P.-Y. Lee, L.-Y. Lin, Synthesizing nickel-based transition bimetallic oxide via nickel precursor-free hydrothermal synthesis for battery supercapacitor hybrid devices, *Journal of colloid and interface science*, 538 (2019) 297-307.
- [19] X. Jiang, Z. Wang, Q. Deng, F. Zhang, F. You, C. Yao, Zinc-Doped Nickel Oxide Hollow Microspheres—Preparation Hydrothermal Synthesis and Electrochemical Properties, *European Journal of Inorganic Chemistry*, 2018 (2018) 4345-4348.
- [20] b. Anandan, V. Rajendran, Morphological and size effects of NiO nanoparticles via solvothermal process and their optical properties, *Materials Science in Semiconductor Processing*, 14 (2011) 43-47.
- [21] Y. Yang, Y. Liang, Z. Zhang, Y. Zhang, H. Wu, Z. Hu, Morphology well-controlled synthesis of NiO by solvothermal reaction time and their morphology-dependent pseudocapacitive performances, *Journal of Alloys and Compounds*, 658 (2016) 621-628.
- [22] N.M. Juibari, A. Eslami, Synthesis of nickel oxide nanorods by Aloe vera leaf extract, *Journal of Thermal Analysis and Calorimetry*, 136 (2019) 913-923.
- [23] A. Kalam, A.G. Al-Sehemi, A.S. Al-Shihri, G. Du, T. Ahmad, Synthesis and characterization of NiO nanoparticles by thermal decomposition of nickel linoleate and their optical properties, *Materials Characterization*, 68 (2012) 77-81.
- [24] M. Grdeń, K. Klimek, EQCM studies on oxidation of metallic nickel electrode in basic solutions, *Journal of Electroanalytical Chemistry*, 581 (2005) 122-131.
- [25] M. Salavati-Niasari, N. Mir, F. Davar, A novel precursor in preparation and characterization of nickel oxide nanoparticles via thermal decomposition approach, *Journal of Alloys and Compounds*, 493 (2010) 163-168.
- [26] B. Vidhyadharan, N.K.M. Zain, I.I. Misnon, R.A. Aziz, J. Ismail, M.M. Yusoff, R. Jose, High performance supercapacitor electrodes from electrospun nickel oxide nanowires, *Journal of Alloys and Compounds*, 610 (2014) 143-150.
- [27] C. Shao, X. Yang, H. Guan, Y. Liu, J. Gong, Electrospun nanofibers of NiO/ZnO composite, *Inorganic Chemistry Communications*, 7 (2004) 625-627.
- [28] H. Guan, C. Shao, S. Wen, B. Chen, J. Gong, X. Yang, Preparation and characterization of NiO nanofibres via an electrospinning technique, *Inorganic Chemistry Communications*, 6 (2003) 1302-1303.
- [29] S.F. Anis, B.S. Lalia, A.O. Mostafa, R. Hashaikeh, Electrospun nickel–tungsten oxide composite fibers as active electrocatalysts for hydrogen evolution reaction, *Journal of materials science*, 52 (2017) 7269-7281.
- [30] S.-j. Kim, H. Jung, C. Lee, M.H. Kim, Y. Lee, Comparative Study on Hydrogen Evolution Reaction Activity of Electrospun Nanofibers with Diverse Metallic Ir and IrO<sub>2</sub> Composition Ratios, *ACS Sustainable Chemistry & Engineering*, 7 (2019) 8613-8620.
- [31] M. Zhu, J. Sun, C. Li, C. Han, Y. Shan, J. He, J. Jia, W. Wu, G. Yang, Electrospun SiO<sub>2</sub>/WO<sub>3</sub>/NiWO<sub>4</sub> decorated carbon nanofibers for an efficient electrocatalytic hydrogen evolution, *Fullerenes, Nanotubes and Carbon Nanostructures*, 27 (2019) 506-513.
- [32] Z.G. Shiri, S.M. Zebarjad, K. Janghorban, A study on the role of electrospinning parameters on the morphology of nickel oxide nano-belts, *Materials Research Express*, (2019).
- [33] N. Dharmaraj, H. Park, C. Kim, H. Kim, D. Lee, Nickel titanate nanofibers by electrospinning, *Materials chemistry and physics*, 87 (2004) 5-9.

- [34] A.A. Nada, M. Nasr, R. Viter, P. Miele, S.p. Roualdes, M. Bechelany, Mesoporous ZnFe<sub>2</sub>O<sub>4</sub>@ TiO<sub>2</sub> nanofibers prepared by electrospinning coupled to PECVD as highly performing photocatalytic materials, *The Journal of Physical Chemistry C*, 121 (2017) 24669-24677.
- [35] A.A. Nada, M.F. Bekheet, R. Viter, P. Miele, S. Roualdes, M. Bechelany, BN/GdxTi (1-x) O (4-x)/2 nanofibers for enhanced photocatalytic hydrogen production under visible light, *Applied Catalysis B: Environmental*, 251 (2019) 76-86.
- [36] A. Barhoum, K. Pal, H. Rahier, H. Uludag, I.S. Kim, M. Bechelany, Nanofibers as new-generation materials: From spinning and nano-spinning fabrication techniques to emerging applications, *Applied Materials Today*, 17 (2019) 1-35.
- [37] D. Gugulothu, A. Barhoum, S.M. Afzal, B. Venkateshwarlu, H. Uludag, Structural Multifunctional Nanofibers and their Emerging Applications, *Handbook of Nanofibers*, A. Barhoum, M. Bechelany, and A. Makhoulouf, Editors. 2018, Springer, (2018) 1-41.
- [38] L. Haichao, L. Haoyi, M. Bubakir, Y. Weimin, A. Barhoum, Engineering nanofibers as electrode and membrane materials for batteries, supercapacitors, and fuel cells, *Handbook of Nanofibers*; Springer International Publishing: Cham, Switzerland, (2018) 1-27.
- [39] A. Shalan, A. Barhoum, A. Elseman, M. Rashad, M. Lira-Cantú, *Handbook of Nanofibers*, in, Springer: Cham, Switzerland, 2018.
- [40] X. Chen, L. Cheng, H. Li, A. Barhoum, Y. Zhang, X. He, W. Yang, M.M. Bubakir, H. Chen, Magnetic nanofibers: unique properties, fabrication techniques, and emerging applications, *ChemistrySelect*, 3 (2018) 9127-9143.
- [41] A. Khalil, R. Hashaikeh, Electrospinning of nickel oxide nanofibers: Process parameters and morphology control, *Materials Characterization*, 95 (2014) 65-71.
- [42] A. Khalil, R. Hashaikeh, Electrospun nickel oxide nanofibers: Microstructure and surface evolution, *Applied Surface Science*, 357 (2015) 1333-1342.
- [43] I.S. Chronakis, Novel nanocomposites and nanoceramics based on polymer nanofibers using electrospinning process—a review, *Journal of materials processing technology*, 167 (2005) 283-293.
- [44] J. Cheng, B. Wang, M. Zhao, F. Liu, X. Zhang, Nickel-doped tin oxide hollow nanofibers prepared by electrospinning for acetone sensing, *Sensors and Actuators B: Chemical*, 190 (2014) 78-85.
- [45] H.H. El-Maghrabi, A. Barhoum, A.A. Nada, Y.M. Moustafa, S.M. Seliman, A.M. Youssef, M. Bechelany, Synthesis of mesoporous core-shell CdS@ TiO<sub>2</sub> (0D and 1D) photocatalysts for solar-driven hydrogen fuel production, *Journal of Photochemistry and Photobiology A: Chemistry*, 351 (2018) 261-270.
- [46] Q. Ding, M. Liu, Y.-E. Miao, Y. Huang, T. Liu, Electrospun nickel-decorated carbon nanofiber membranes as efficient electrocatalysts for hydrogen evolution reaction, *Electrochimica Acta*, 159 (2015) 1-7.
- [47] X. Zou, Y. Zhang, Noble metal-free hydrogen evolution catalysts for water splitting, *Chemical Society Reviews*, 44 (2015) 5148-5180.
- [48] A. Chinnappan, J. Dongxiao, W. Jayathilaka, C. Baskar, X. Qin, S. Ramakrishna, Facile synthesis of electrospun C@ NiO/Ni nanofibers as an electrocatalyst for hydrogen evolution reaction, *International Journal of Hydrogen Energy*, 43 (2018) 15217-15224.
- [49] M. Wu, L. Fan, R. Ma, J. Zhu, S. Gu, T. Wang, D. Gong, Z. Xu, B. Lu, NiO and CrO<sub>3</sub> double surface-decorate Ni nanofibers for hydrogen evolution reduction, *Materials Letters*, 182 (2016) 15-18.
- [50] J. Bao, X. Zhang, B. Fan, J. Zhang, M. Zhou, W. Yang, X. Hu, H. Wang, B. Pan, Y. Xie, Ultrathin spinel-structured nanosheets rich in oxygen deficiencies for enhanced electrocatalytic water oxidation, *Angewandte Chemie International Edition*, 54 (2015) 7399-7404.
- [51] P. He, X. Yi, Y. Ma, W. Wang, F. Dong, L. Du, H. Liu, Effect of Gd<sub>2</sub>O<sub>3</sub> on the hydrogen evolution property of nickel-cobalt coatings electrodeposited on titanium substrate, *Journal of Physics and Chemistry of Solids*, 72 (2011) 1261-1264.

- [52] P. Sivasakthi, S. Premlatha, G.R. Babu, M. Chandrasekaran, Pulse electrodeposited Ni-CeO<sub>2</sub>Gd doped nanocomposite on copper foam as an electrocatalysts for hydrogen evolution reaction, *International Journal of Hydrogen Energy*, 42 (2017) 4741-4750.
- [53] A. Barhoum, H.H. El-Maghrabi, I. Iatsunskyi, E. Coy, A. Renard, C. Salameh, M. Weber, S. Sayegh, A.A. Nada, S. Roualdes, Atomic layer deposition of Pd nanoparticles on self-supported carbon-Ni/NiO-Pd nanofiber electrodes for electrochemical hydrogen and oxygen evolution reactions, *Journal of Colloid and Interface Science*, 569 (2020) 286-297.
- [54] Y. Xian Yan, T. Ahmad, X. Zhang, T. Liang, S.U. Rehman, M. Manzoor, W. Liu, M.A. Basit, Microstructure, hardness and corrosion behavior of Ni-Ti alloy with the addition of rare earth metal oxide (Gd<sub>2</sub>O<sub>3</sub>), *Materials Research Express*, 6 (2019).
- [55] P. Ilanchezhian, G. Mohan Kumar, S. Tamilselvan, T.W. Kang, D.Y. Kim, Highly efficient overall water splitting performance of gadolinium-indium-zinc ternary oxide nanostructured electrocatalyst, *International Journal of Energy Research*, (2020).
- [56] J. Rodríguez-Carvajal, Recent developments of the program FULLPROF, Commission on powder diffraction (IUCr). Newsletter, 26 (2001) 12-19.
- [57] L. Finger, D. Cox, A. Jephcoat, A correction for powder diffraction peak asymmetry due to axial divergence, *Journal of Applied Crystallography*, 27 (1994) 892-900.
- [58] H. Kedesdy, A. Drukalsky, X-Ray Diffraction Studies of the Solid State Reaction in the NiO-ZnO System, *Journal of the American Chemical Society*, 76 (1954) 5941-5946.
- [59] R.D. Shannon, Revised effective ionic-radii and systematic studies of interatomic distances in halides and chalcogenides, *Acta Crystallogr A*, 32 (1976) 751-767.
- [60] M.F. Bekheet, L. Dubrovinsky, A. Gurlo, Compressibility and structural stability of spinel-type MnIn<sub>2</sub>O<sub>4</sub>, *Journal of Solid State Chemistry*, 230 (2015) 301-308.
- [61] M.F. Bekheet, L. Schlicker, A. Doran, K. Siemensmeyer, A. Gurlo, Ferrimagnetism in manganese-rich gallium and aluminium spinels due to mixed valence Mn<sup>2+</sup>-Mn<sup>3+</sup> states, *Dalton Transactions*, 47 (2018) 2727-2738.
- [62] D. Varshney, S. Dwivedi, Synthesis, structural, Raman spectroscopic and paramagnetic properties of Sn doped NiO nanoparticles, *Superlattices and Microstructures*, 86 (2015) 430-437.
- [63] S. Hazarika, P.S. Behera, D. Mohanta, R. Nirmala, Magnetocaloric effect of Gd<sub>2</sub>O<sub>3</sub> nanorods with 5% Eu-substitution, *Applied Surface Science*, 491 (2019) 779-783.
- [64] D.H. Reneker, I. Chun, Nanometre diameter fibres of polymer, produced by electrospinning, *Nanotechnology*, 7 (1996) 216.
- [65] Z.-M. Huang, Y.-Z. Zhang, M. Kotaki, S. Ramakrishna, A review on polymer nanofibers by electrospinning and their applications in nanocomposites, *Composites science and technology*, 63 (2003) 2223-2253.
- [66] J.T. McCann, D. Li, Y. Xia, Electrospinning of nanofibers with core-sheath, hollow, or porous structures, *Journal of Materials Chemistry*, 15 (2005) 735-738.
- [67] C. Wu, S. Deng, H. Wang, Y. Sun, J. Liu, H. Yan, Preparation of novel three-dimensional NiO/ultrathin derived graphene hybrid for supercapacitor applications, *ACS applied materials & interfaces*, 6 (2014) 1106-1112.
- [68] D. Raiser, J. Deville, Study of XPS photoemission of some gadolinium compounds, *Journal of electron spectroscopy and related phenomena*, 57 (1991) 91-97.
- [69] J. Zhang, D. Zeng, Q. Zhu, J. Wu, Q. Huang, C. Xie, Effect of nickel vacancies on the room-temperature NO<sub>2</sub> sensing properties of mesoporous NiO nanosheets, *The Journal of Physical Chemistry C*, 120 (2016) 3936-3945.
- [70] D. Joshi, S. Nayak, A. Kumar, A. Mohanta, D. Pamu, S. Thota, Peculiarities of the temperature dependence of electron spin resonance and Raman studies of Zn<sub>1-x</sub>Ni<sub>x</sub>O/NiO two-phase nanocomposites, *Journal of Applied Physics*, 119 (2016) 074303.

- [71] G. Dixit, J.P. Singh, R. Srivastava, H. Agrawal, Magnetic resonance study of Ce and Gd doped NiFe<sub>2</sub>O<sub>4</sub> nanoparticles, *Journal of Magnetism and Magnetic Materials*, 324 (2012) 479-483.
- [72] H.k. Gustafsson, M. Ahrén, F. Söderlind, J.M. Córdoba Gallego, P.-O. Käll, P. Nordblad, P.-O. Westlund, K. Uvdal, M. Engström, Magnetic and Electron Spin Relaxation Properties of (Gd<sub>x</sub>Y<sub>1-x</sub>)<sub>2</sub>O<sub>3</sub> (0 ≤ x ≤ 1) Nanoparticles Synthesized by the Combustion Method. Increased Electron Spin Relaxation Times with Increasing Yttrium Content, *The Journal of Physical Chemistry C*, 115 (2011) 5469-5477.
- [73] M. Rubinstein, R. Kodama, S.A. Makhlof, Electron spin resonance study of NiO antiferromagnetic nanoparticles, *Journal of magnetism and magnetic materials*, 234 (2001) 289-293.
- [74] A. Davidson, J. Tempere, M. Che, H. Roulet, G. Dufour, Spectroscopic studies of nickel (II) and nickel (III) species generated upon thermal treatments of nickel/ceria-supported materials, *The Journal of Physical Chemistry*, 100 (1996) 4919-4929.
- [75] V. Singh, M. Seehra, Temperature and size dependence of electron magnetic resonance spectra of Ni nanoparticles embedded in an amorphous SiO<sub>2</sub> matrix, *Journal of Physics: Condensed Matter*, 21 (2009) 456001.
- [76] C. Mitsumata, S. Tomita, M. Hagiwara, K. Akamatsu, Electron magnetic resonance in interacting ferromagnetic-metal nanoparticle systems: experiment and numerical simulation, *Journal of Physics: Condensed Matter*, 22 (2009) 016005.
- [77] W. Sheng, M. Myint, J.G. Chen, Y. Yan, Correlating the hydrogen evolution reaction activity in alkaline electrolytes with the hydrogen binding energy on monometallic surfaces, *Energy & Environmental Science*, 6 (2013) 1509-1512.
- [78] J. Greeley, T.F. Jaramillo, J. Bonde, I. Chorkendorff, J.K. Nørskov, Computational high-throughput screening of electrocatalytic materials for hydrogen evolution, *Nature materials*, 5 (2006) 909-913.
- [79] S. Oh, H. Kim, Y. Kwon, M. Kim, E. Cho, H. Kwon, Porous Co-P foam as an efficient bifunctional electrocatalyst for hydrogen and oxygen evolution reactions, *Journal of Materials Chemistry A*, 4 (2016) 18272-18277.
- [80] R. Zhang, H. Wei, W. Si, G. Ou, C. Zhao, M. Song, C. Zhang, H. Wu, Enhanced electrocatalytic activity for water splitting on NiO/Ni/carbon fiber paper, *Materials*, 10 (2017) 15.
- [81] S. Lu, M. Hummel, Z. Gu, Y. Gu, Z. Cen, L. Wei, Y. Zhou, C. Zhang, C. Yang, Trash to treasure: A novel chemical route to synthesis of NiO/C for hydrogen production, *International Journal of Hydrogen Energy*, 44 (2019) 16144-16153.